

# Euler/Navier-Stokes couplings for multiscale aeroacoustic problems

Michel Borrel, Laurence Halpern & Juliette Ryan

**Abstract** We present in this paper two Euler/Navier-Stokes couplings for multiscale aeroacoustic problems based on a Discontinuous Galerkin method: the first coupling concerns an interface coupling between adjacent domains, the second coupling concerns a coupling in volume and interface between overlapping domains. In both cases, each domain provide a donor field to the other domain. After a numerical study of the convergence of the precision of the method, these couplings are compared on a 2D test case of a flow around a cylinder and the noise generated.

**Key words:** CFD, CAA, coupling method, multiscale problem, Navier-Stokes, Euler, Euler in perturbation, Discontinuous Galerkin method

## 1 Introduction

In the last few years numerical aeroacoustics have undergone a very rapid evolution due to the emergence of direct simulations of sound emitted by flows, and in particular turbulent flows. However, the computational cost of these computations raise the question of the coupling between LES and acoustics or in other words between the Navier-Stokes and the Euler computations, especially if we want to take into account the multiscale aspect, both in space and time, of the problem.

In this paper Euler/Navier-Stokes coupling approaches are presented . A first type is a coupling between aerodynamics and acoustics first presented at ICCFD 2010 [3] . It is based on earlier work on Schwarz waveform relaxation methods , developed for time-dependent advection - diffusion - reaction. These methods are domain decomposition algorithms. They consist in solving the equations alternatively in each subdomain, and transmitting the necessary information through differential space-time transmission conditions, see for example [2]. They allow for different discretization in different subdomains, see [1], even in a non-conformal manner [13]. They can potentially extend to coupling different models in different zones,

---

Michel Borrel e-mail: borrel@onera.fr, Juliette Ryan e-mail: ryan@onera.fr  
ONERA, BP72 - 29 avenue de la Division Leclerc, FR-92322, CHATILLON CEDEX, FRANCE,

Laurence Halpern e-mail: halpern@math.univ-paris13.fr  
LAGA, Université Paris XIII and CNRS, 99 avenue J.B. Clément, 93430 Villeteuse, FRANCE

see [10], and are therefore well-adapted to our purpose. In this first approach, the coupling is performed exactly at the interface between the Navier-Stokes and the Euler meshes, which are non-conformal both in space and time due to the multi-scale aspect of the physics under consideration.

Another coupling method could be based on an embedded grid strategy of Chimera type where the coupling is performed through a volume interpolation of the Navier-Stokes solution on the Euler grid which gives the source terms of the Euler equations in perturbation [8]. A second type of exchange (Euler towards Navier-Stokes) is done through the immersed boundaries using the same type of conditions as the first approach. This coupling, in fact, can be viewed as a sequel of our previous work on AMR [6], [17].

In Section 2 we recall the governing equations and we detail the Discontinuous Galerkin (DG) scheme used for solving

- a) the Navier-Stokes equations (CFD)
- b) the Euler equations or the Euler equations in perturbation (CAA).

We have formulated in [4] a new Discontinuous Galerkin scheme (EDG) for the viscous term that easily applies to either structured or non structured discretizations. The EDG method is closely related to the recovery method proposed by Van Leer *et al.* [23]-[24], though it is simpler to implement. Special attention must be paid to the multi-scale aspect requiring highly non conforming space-time discretization for which the discontinuous Galerkin approach is particularly well adapted.

A detailed description of the two couplings is presented in Section 3. Both approximations seem equally attractive. 2D numerical results are presented in 4. The test case is that of the low-Reynolds subsonic flow around a cylinder.

## 2 Numerical Discretization

### 2.1 Governing equations

The governing equations to be solved are the Euler and the Navier-Stokes equations in 2D for a compressible flow which express conservation of mass, momentum and energy

$$\partial_t \mathcal{W} + \nabla \cdot \mathbf{F}(\mathcal{W}) - \nabla \cdot \mathbf{F}^D(\mathcal{W}, \nabla \mathcal{W}) = \mathbf{0} \quad (1)$$

where  $\mathcal{W} = (\rho, \rho \vec{U}, \rho E)$  is the conservation variable vector with classical notations,  $\mathbf{F}$  represents the Euler fluxes:

$$\mathbf{F} = \left( \rho \vec{U}, \rho \vec{U} \otimes \vec{U} + pI, \vec{U}(\rho E + p) \right) \quad (2)$$

and  $\mathbf{F}^D$  represents the diffusion and heat fluxes of the Navier-Stokes equations:

$$\mathbf{F}^D = \left( 0, \bar{\tau}, \bar{\tau} \cdot \vec{U} + \lambda \nabla T \right). \quad (3)$$

Above  $\rho$  is the density,  $\vec{U} = (u, v)$  the velocity,  $\bar{\tau}$  the shear stress tensor,  $p$  the pressure,  $T$  the temperature,  $E = e + (u^2 + v^2)/2$  the total energy with  $e$  the specific internal energy and  $\lambda$  is the thermal conductivity. We assume the gas to be calorically perfect, with the heat capacities  $c_v, c_p$  and the Prandtl number constant ( $Pr = 0.72$ ). So, we can express  $e = c_v T$  and  $\lambda = c_p \mu / Pr$  where  $\mu$  is the dynamic viscous coefficient given by Sutherland's law. The pressure  $p$  is given with the perfect polytropic gas state law  $p = \rho R T = (\gamma - 1) \rho e$  with  $R = c_p - c_v$  the specific gas constant and  $\gamma$  the specific heat ratio ( $\gamma = c_p / c_v = 1.4$ ). The Newtonian fluid hypothesis and the Stokes relation define the shear stress tensor in terms of the dynamic viscosity coefficient  $\mu$  and the gradient of the velocity:

$$\bar{\tau} = \mu \left( \nabla \vec{U} + (\nabla \vec{U})^T - \frac{2}{3} (\nabla \cdot \vec{U}) \bar{I} \right). \quad (4)$$

## 2.2 DG formulation

The Euler or the Navier-Stokes equations are solved in a domain  $\Omega$  discretized by either a Cartesian or an unstructured triangular grid  $\mathcal{T}_h = \bigcup \Omega_i$  and the associated function space  $V_h$

$$V_h = \{ \phi \in L^2(\Omega) \mid \phi / \Omega_i \in P_k \} \quad (5)$$

where  $P_k$  is the space of polynomials of degree  $k$ .

The DG formulation based on a weak formulation after a first integration by parts is of the form : find  $\mathcal{W}^h$  in  $(V_h)^4$  such that for all  $\Omega_i$  in  $\mathcal{T}_h$ ,

$$\forall \phi \in V_h, \quad \int_{\Omega_i} \partial_t \mathcal{W}_h \phi \, dx = \int_{\Gamma_i} (\mathbf{F}_h - \mathbf{F}_h^D) \phi \, d\gamma - \int_{\Omega_i} (\mathbf{F}_h - \mathbf{F}_h^D) \nabla \phi \, dx. \quad (6)$$

Here, the numerical fluxes  $\mathbf{F}_h, \mathbf{F}_h^D$  and  $\mathcal{W}_h$  are approximations of  $\mathbf{F}, \mathbf{F}^D$  and  $\mathcal{W}$ . The Euler fluxes  $\mathbf{F}$  are classically determined using the LLF (Local Lax-Friedrichs) or HLLC fluxes ([21]); we will detail in the next section the viscous flux computation through the EDG method.

If we neglect locally the dependency of  $\mu$  on temperature, the viscous term  $\mathbf{F}^D$  can be split into a linear and a nonlinear part,

$$\mathbf{F}^D = \mathcal{L}(\nabla \vec{U}, \nabla T) + \mathcal{N}(\vec{U} \cdot \tau). \quad (7)$$

A second integration by parts can be done on the linear part  $\mathcal{L}(\nabla \vec{U}, \nabla T)$  thus giving the following formulation,

$$\forall \phi \in V_h, \quad \int_{\Omega_i} \partial_t \mathcal{W}_h \phi \, dx = \int_{\Gamma_i} (\mathbf{F}_h - \mathbf{F}_h^D + \mathcal{L}(\vec{U}, T)) \phi \, d\gamma - \int_{\Omega_i} (\mathbf{F}_h + \mathcal{L}(\vec{U}, T) - \mathcal{N}(\vec{U} \cdot \boldsymbol{\tau})) \nabla \phi \, dx. \quad (8)$$

Finally, we take in the space  $V_h$  a basis built locally with the Legendre polynomials, this basis being orthogonalized for triangle elements. So, this formulation results in a system of coupled ordinary differential equations of the form

$$\mathcal{M} \partial_t \mathbf{W}_h = \mathbf{R}(\mathbf{W}_h) \quad (9)$$

where  $\mathbf{W}_h$  is the vector containing the degrees of freedom (DOF) associated to  $\mathcal{W}_h$  expressed in a basis of  $V_h$  and  $\mathcal{M}$  the mass matrix, which is diagonal, while  $\mathbf{R}$  are the residuals which are nonlinear functions of  $\mathbf{W}_h$ . We have chosen the explicit time stepping RK3 of Shu-Osher [20] to solve (Eq. 9). As usual, the time step is subject to a CFL-like restriction.

### 2.3 The EDG method

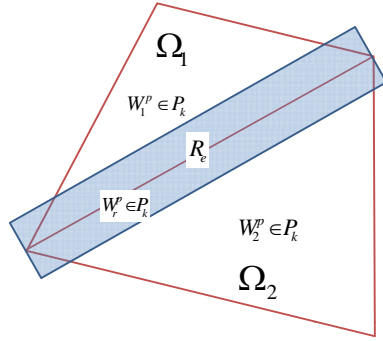


**Fig. 1** Definition of the elastoplast element (color area) overlapping the interface between two triangular elements  $\Omega_1, \Omega_2$ .

We are only concerned here with the diffusion terms. The simple idea of the EDG method is to regularize locally the discontinuous solution  $\mathcal{W}_h$  over each edge using an  $L^2$  projection in a rectangular interpolation element  $E$  overlapping this edge (see Fig. 1). The basis in  $E$  of the same order  $k$  as the DG basis defined in the elements, using on either side of the edge an equal number of Gauss quadrature points, which number provides at least the order of the original solution.

More precisely, for any interface  $\Gamma$  between elements  $\Omega_1$  and  $\Omega_2$ , the regularized solution in  $E$  is expanded in the DG- $P_k$  basis:

$$\mathcal{W}_E = \sum_P W_E^P \phi_E^P \quad (10)$$

where  $\phi_E^P$  represents the DG- $P_k$  basis functions and  $W_E^P$  the unknowns which are computed by:

$$W_E^p = \frac{1}{(\phi_E^p, \phi_E^p)_E} \left( \int_{\Omega_1 \cap E} W_1^p \phi_E^p dx + \int_{\Omega_2 \cap E} W_2^p \phi_E^p dx \right). \quad (11)$$

Above,  $W_1^p$  and  $W_2^p$  are the local DG- $P_k$  solutions in  $\Omega_1$  and  $\Omega_2$ ,  $(\bullet, \bullet)_E$  is the  $L^2$  product in  $E$ ,

$$\forall \phi, \psi \in L^2(\Omega) \quad (\phi, \psi)_E = \int_E \phi \psi dx \quad (12)$$

All integrals are numerically computed using a  $n$ -point Gaussian quadrature rule, such that  $2 * n - 1 \geq k$ ,  $k$  order of the local DG formulation.

This idea of rectangular interpolation element at the interfaces will be generalized to the Euler/Navier-Stokes coupling in a Cartesian / triangular framework.

## 2.4 Limiters

The use of limiters is one of the drawback of the DG approach. Hopefully, we generally don't need them for CAA, but it is not the case for the computation of vortical flows. So, we need to restrict their use. Thus in this paper, our results for the cylinder flow will be for a Reynolds number based on the diameter of 500 for which limiters are not needed.

## 3 Euler/Navier-Stokes Couplings

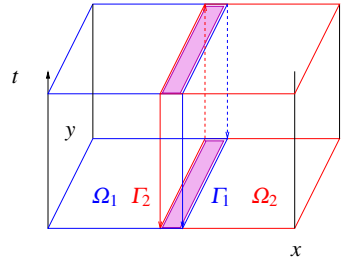
### 3.1 Adjacent domain coupling

#### 3.1.1 Schwarz waveform relaxation methods

These methods are based on Schwarz domain decomposition algorithms, invented by H.A. Schwarz in 1870 [19]. In order to solve a Laplace equation in the domain  $\Omega$ , it is split into two subdomains with overlap  $\Omega_1$  and  $\Omega_2$ , in which the equation is solved alternatively. Exchange of information is made on the boundaries by exchange of Dirichlet values. This algorithm has been extended by P.L. Lions to nonoverlapping subdomains using different transmission conditions, such as Robin conditions [15]. For an extension to evolution problem, we couple it to a waveform relaxation algorithm, which is an extension both of the Picard's "approximations successives" and relaxation methods for algebraic systems, due to Lelarmsee [14]. Versions with Dirichlet or optimized Robin transmission conditions have been designed in [2] for the unsteady heat equation with prescribed Dirichlet boundary conditions and initial data:

$$\begin{cases} \partial_t u - v \Delta u = f & \text{in } \Omega \times [0, T] \\ u(x, 0) = u_0(x) & \text{in } \Omega \\ u = g & \text{on } \partial\Omega \end{cases} \quad (13)$$

where  $u$  is the temperature,  $v$  is the constant diffusive coefficient and  $\Delta$  represents the Laplace operator. A parallel version of the Schwarz waveform relaxation algorithm can be generalized from a decomposition in two domains  $\Omega = \Omega_1 \cup \Omega_2$  associated with two spatial operators  $\mathcal{L}_1$  and  $\mathcal{L}_2$ , and two interface operators  $\mathcal{B}_1$  and  $\mathcal{B}_2$  (called the transmission conditions) as



$$\begin{cases} \partial_t u_1^k - \mathcal{L}_1 u_1^k = f & \text{in } \Omega_1 \times (0, T), \\ u_1^k(\cdot, 0) = u_0 & \text{in } \Omega_1, \\ \mathcal{B}_1 u_1^k = \mathcal{B}_1 u_2^{k-1} & \text{on } \Gamma_1 \times (0, T), \\ u_1^k = g & \text{on } (\partial\Omega_1 - \Gamma_1) \times (0, T), \end{cases}$$

$$\begin{cases} \partial_t u_2^k - \mathcal{L}_2 u_2^k = f & \text{in } \Omega_2 \times (0, T), \\ u_2^k(\cdot, 0) = u_0 & \text{in } \Omega_2, \\ \mathcal{B}_2 u_2^k = \mathcal{B}_2 u_1^k & \text{on } \Gamma_2 \times (0, T), \\ u_2^k = g & \text{on } (\partial\Omega_2 - \Gamma_2) \times (0, T). \end{cases}$$

If we take for the transmission operators  $\mathcal{B}_j = Id$ , an overlap between the domains is necessary. Optimal transmission conditions (Robin conditions) can be written for the heat equation as

$$\mathcal{B}_j = v \partial_{n_j} + p, \quad j = 1, 2 \quad (14)$$

where  $n_j$  is the unit normal exterior to  $\Gamma_j$ . The relaxation parameter  $p$  is determined asymptotically as a function of the physical parameters, the size of the space-time domains and the mesh parameters (see [2]). In that case we can use adjacent domains without overlap.

We propose in this paper to extend this algorithm for systems and more precisely to take for operators  $\mathcal{L}_1$  and  $\mathcal{L}_2$  the Navier-Stokes and the Euler operators respectively. The Dirichlet or the Robin conditions at the interface will be applied in through an integral formulation computed with the relevant Gauss nodes. Notice that  $v = 0$  for the Euler operator and that  $v$  is no longer a constant for the Navier-Stokes operator.

### 3.1.2 Implementation

General technique: to compute Euler fluxes (resp. viscous fluxes) at interface boundaries, 3 gauss point values are needed on the interface (resp. 9 gauss point values in the EDG cell). All necessary DOF are sent to the other domain asynchronously so

that fluxes can be computed in a transparent way, whether there are rectangular or triangular elements.

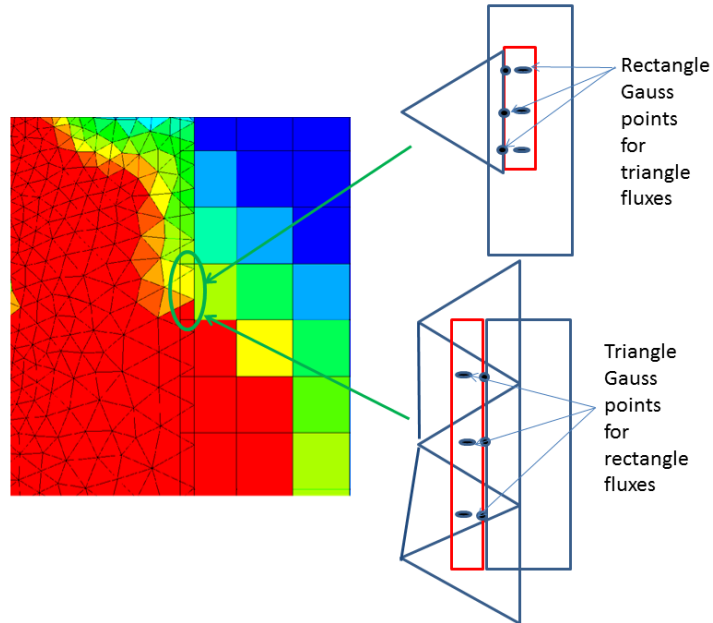


**Fig. 2** Definition of the coupling in space.

We have to couple the Schwarz sub-iterations (parameter  $k$  in the equations above) with the time stepping (RK3) used in the domains  $\Omega_1$  and  $\Omega_2$ , but with different time steps. We want to use a parallel algorithm. Time windows are defined in such a way that time coincides on the two domains at the end of the time window for both domains. Then the local CFL number is adjusted so that  $m$  time steps are performed in domain  $\Omega_1$  and  $n$  time steps are performed in domain  $\Omega_2$  within each time window. Fig. 3 shows an example of a whole Schwarz iteration.

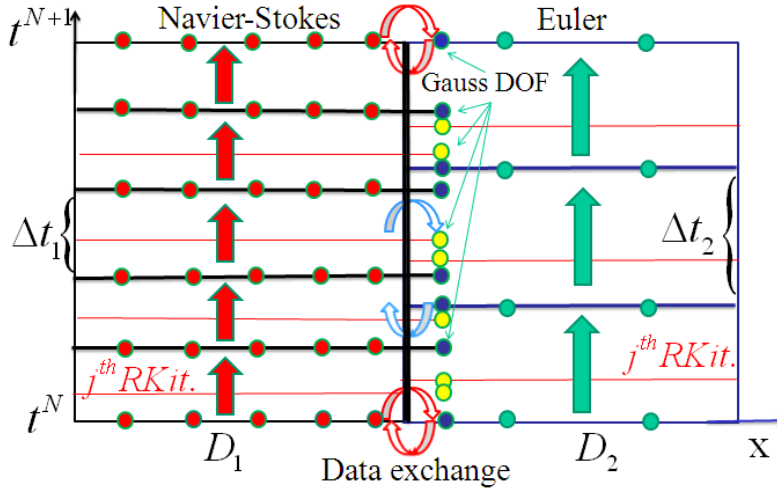


**Fig. 3** Sketch of one Schwarz iteration in a time window defined at the interface between two domains  $D_1, D_2$ . Here, the dots represent the DOF, the vertical arrows represent the full time steps, the horizontal red lines represents the  $j^{\text{th}}$  RK iterations and the horizontal arrows represent the exchange data for the parallel computing. The Gauss DOF, which are to be interpolated at Gauss integration nodes in the domain  $D_2$ , are only represented for the domain  $D_1$ . Notice that the blue and yellow Gauss DOF are interpolated in time separately.

Domains proceed in time independently, using at first predefined interface values. At the end of the time window, domains exchange their newly computed boundary cells values for all time steps (including sub times for the Runge Kutta scheme) and a new time march is carried out with updated interface values. This iterative procedure is repeated till solution ceases to vary. This method allows for different time steps and different space interface discretization as received values from other domains can be interpolated and projected on the local time-space grid. In time, when enough time steps exist per window, different quadratic interpolations are used to interpolate the DOF in the ghost element. Asynchronous exchange data are performed inside the time window with few impact on the parallel computing time.

Notice that a non iterative algorithm could perhaps be devised as in [22] using an ADER procedure, but as two or three iterations are generally sufficient to converge we take benefit of a very general and simple algorithm.

### 3.2 Embedded domain coupling

#### 3.2.1 Euler equations in perturbation

If we consider the acoustics as a linear perturbation of the mean flow of the CFD flowfield, the governing equations of the CAA are the linearized Euler equations. An important issue of the coupling between the CFD and the CAA is then to define the mean flow. In fact, as we want to limit the CFD domain as much as possible, the coupling area (where Navier-Stokes and Euler are both defined) is located in a zone where the nonlinear effects are very important and the linearized Euler equations are no more relevant within a fully coupled approach. In that context, the Euler equations in perturbation open the door to an other interesting possibility to a full Navier-Stokes computation.

Here, two overlapping domains are considered  $G_{NS}$  and  $G_{CAA}$  with  $G_{NS}$  completely embedded in  $G_{CAA}$ . On  $G_{NS}$  is computed a Navier-Stokes solution  $\mathcal{W}_{NS}$ .

$$\partial_t \mathcal{W}_{NS} + \nabla \cdot \mathbf{F}(\mathcal{W}_{NS}) - \nabla \cdot \mathbf{F}^D(\mathcal{W}_{NS}, \nabla \mathcal{W}_{NS}) = \mathbf{0} \quad (15)$$

with the same notations as in (Eq. 1).

On  $G_{CAA}$ , the following decomposition is used :  $\mathcal{W} = \mathcal{W}_0 + \mathcal{W}'$  where  $\mathcal{W}$  satisfies the Navier-Stokes equations :

$$\partial_t \mathcal{W} + \nabla \cdot \mathbf{F}(\mathcal{W}) - \nabla \cdot \mathbf{F}^D(\mathcal{W}, \nabla \mathcal{W}) = \mathbf{0} \quad (16)$$

and  $\mathcal{W}_0$  is defined by the assumption that all viscous effects are described with  $\mathcal{W}_0$ , that is :

$$\nabla \cdot \mathbf{F}^D(\mathcal{W}, \nabla \mathcal{W}) = \nabla \cdot \mathbf{F}^D(\mathcal{W}_0, \nabla \mathcal{W}_0) \quad (17)$$

Thus the Euler equations in perturbation can be written:

$$\partial_t \mathcal{W}' + \nabla \cdot \mathbf{F}(\mathcal{W}) = -(\partial_t \mathcal{W}_0 - \nabla \cdot \mathbf{F}^D(\mathcal{W}_0, \nabla \mathcal{W}_0)) = RHS(t) \quad (18)$$

Let  $P$  be the projection operator of the instantaneous values defined on  $G_{NS}$  onto  $G_{CAA}$ .  $\mathcal{W}_0$  is approximated by  $P(\mathcal{W}_{NS})$ . Two approximations based on (Eq. 21) of the right hand side  $RHS(t)$  can be made

$$RHS(t) = \nabla \cdot \mathbf{F}(P(\mathcal{W}_{NS})) \quad (19)$$

$$RHS(t) = P(\nabla \cdot \mathbf{F}(\mathcal{W}_{NS})) \quad (20)$$

#### 3.2.2 Implementation

The implementation of this coupling is very close to the AMR techniques. One time step consists in two stages:

1. The Navier-Stokes solution  $\mathcal{W}_{NS}$  is computed on  $G_{NS}$  and projected onto  $G_{CAA}$  providing  $\mathcal{W}_0$  and the right hand side for (Eq. 18).
2. The euler equations in perturbation are then computed on  $G_{CAA}$  providing new boundary conditions for the Navier-Stokes problem on  $G_{NS}$ .

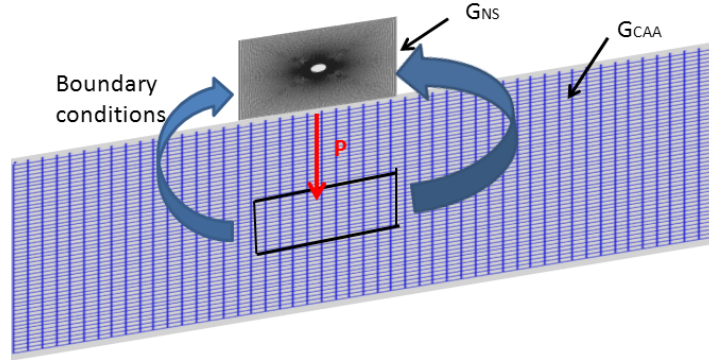


**Fig. 4** Chimera overlapping grids

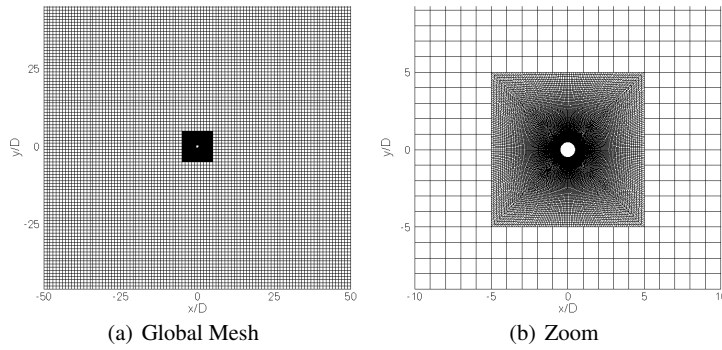


**Fig. 5** Chimera mesh seen from above

## 4 Numerical Results

All computations are  $DG-P_2$ , and no limiters were used for either Euler or Navier-Stokes computations. For both Cartesian and unstructured computations, we used the same functional space  $V_h$ . All triangular grids have been obtained with the free-ware mesh generator Gmsh [12].

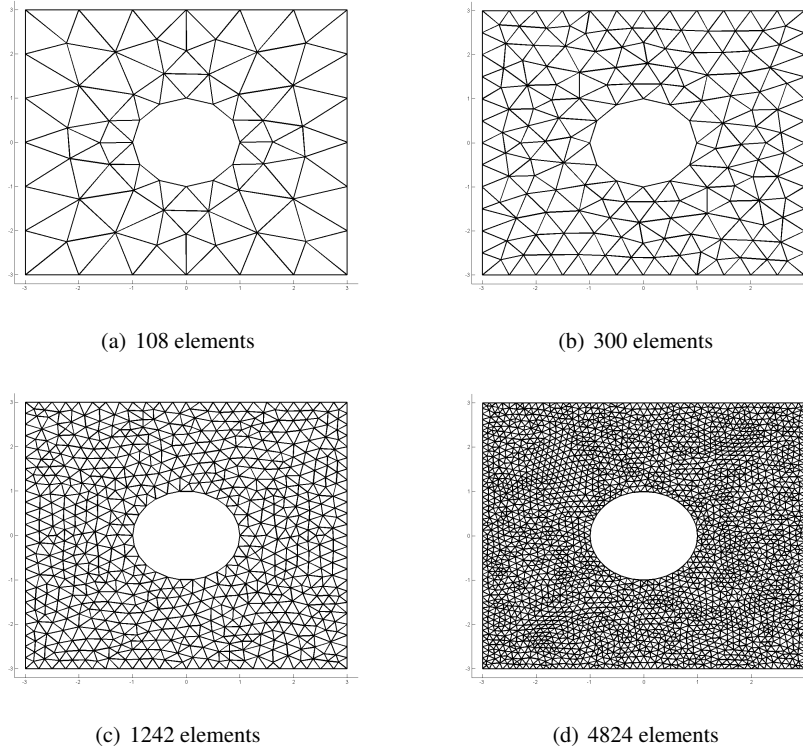


**Fig. 6** Different computational grids for the convergence study

### 4.1 Convergence study

The main issue of a coupling technique is to verify that the numerical algorithm preserves the order of accuracy of the schemes and to define what that means when the coupling concerns the modeling. So, first of all, the experimental order of convergence of the Navier-Stokes with the EDG method is investigated in the case of the inhomogeneous Navier-Stokes equations (Eq. 21) as in Gassner *et al* (see [11]).

$$\partial_t \mathcal{W} + \nabla \cdot \mathbf{F}(\mathcal{W}) - \nabla \cdot \mathbf{D}(\mathcal{W}, \nabla \mathcal{W}) = \mathcal{S} \quad (21)$$

$\mathcal{S}$  is such that

$$\mathcal{W} = \begin{pmatrix} \sin(k(x+y) - \omega t) + c \\ \sin(k(x+y) - \omega t) + c \\ \sin(k(x+y) - \omega t) + c \\ (\sin(k(x+y) - \omega t) + c)^2 \end{pmatrix} \quad (22)$$

is an exact solution to (Eq. 21). Exact boundary conditions are applied by imposing the exact solution at the ghost cell Gauss quadrature points. For the computation, the coefficients were

$$\mu = 0.01 \quad \gamma = 1.4 \quad Pr = 0.72 \quad k = 2.0 \quad \omega = 0.5 \quad c = 4.0 \quad (23)$$

The computational domain is a  $[-3,3] \times [-3,3]$  square where a cylinder centered at the origin with radius equal to one is subtracted. Each mesh is defined by specifying in Gmsh the number of edges on one side of the square (6,12,24,48), providing grids of (108, 300,1242, 4824) cells. The endtime is set to  $t_{end}=1$

In Fig. 6 are shown 3 computational grids obtained with Gmsh [12]. Table 1 presents the  $L^2$  norm of the error for  $p=1$  and  $p=2$  DG discretization.

$N_C$	Rins	p=1 $L^2$ error	$\Theta_{L^2}$	p=2 $L^2$ error	$\Theta_{L^2}$
108	0.22	0.621E-01		0.111E-01	
300	0.13	0.267E-01	2.26	0.353E-02	3.07
1242	0.06	0.498E-02	2.27	0.369E-03	3.06
4824	0.03	0.101E-02	2.19	0.374E-04	3.14

**Table 1** Experimental order of convergence for the EDG scheme.  $N_C$  is the number of cells, Rins is the average radius of inscribed circles, p is the DG order,  $\Theta_{L^2}$  is the order of accuracy.

These results show that that the EDG-P2 scheme converges for the Navier-Stokes equations with the optimal order of accuracy of 3 with error norms that compare well with those of the STE-DG and the BR2-RKDG scheme [11].

### 4.2 Vortex pairing in a time-developing mixing layer at $M_c = 0.2$

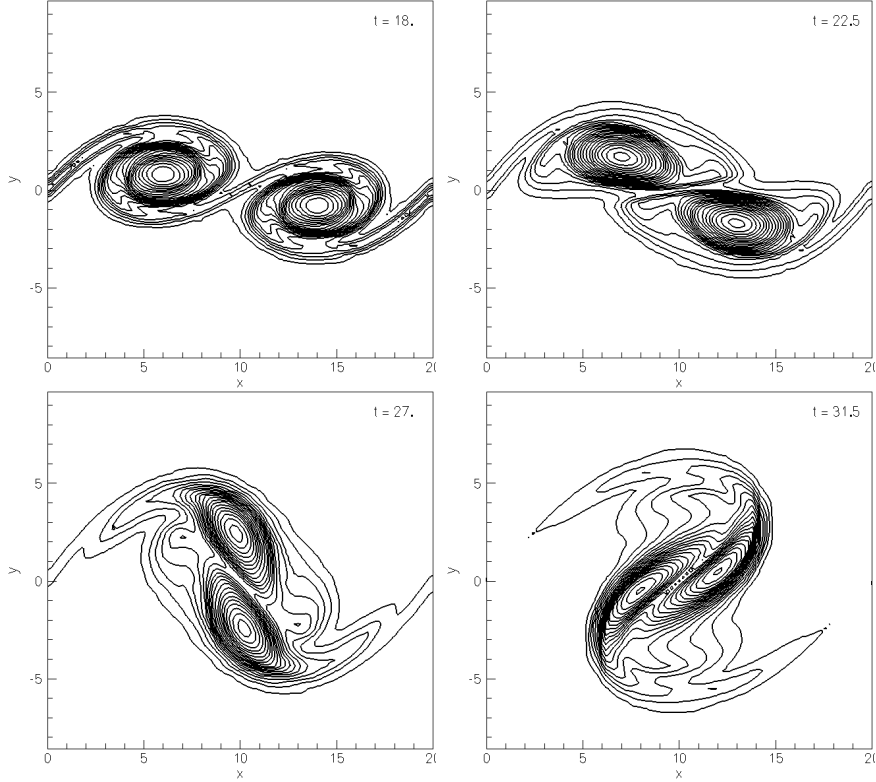


**Fig. 7** Vortex pairing in a time-developing mixing layer at  $Mc=0.2$  : time sequence of the vorticity contours, at times  $t=18, 22.5, 27, 31.5$ , for a  $101 \times 101$  grid (NS computation).

This test case studied vortex growth and pairing in a temporal mixing layer. It has been introduced and studied in detail by Sandham in [18] and later by Yee *et al.* in [25] at a convective Mach number  $M_c = 0.8$ . At a convective Mach number equal to 0.2, diffusion effects are more important and the problem is to compute accurately the viscous effects. Many calculations of this problem can be found in the literature, but our objective here is only to evaluate the EDG scheme for a viscous problem and to show the differences with an inviscid computation.

We set up the base flow as in [18]

$$u = \tanh(2y) \quad (24)$$

with velocities normalized by the velocity jump across the shear layer centered at  $y = 0$  and distances normalized by vorticity thickness

$$\delta_\omega = \frac{\delta u}{(du/dy)_{max}}. \quad (25)$$

The convective Mach number is equal to  $M_c = u_\infty/c_\infty$  and the temperature i.e. the local sound velocity squared is determined from the Crocco-Busemann relation:

$$c^2 = c_\infty^2 + \frac{\gamma-1}{2}(u_\infty^2 - u^2). \quad (26)$$

Equal pressure through the mixing layer is assumed. The Reynolds number defined by the velocity jump, vorticity thickness and kinematic viscosity at the free-stream temperature is set to 200 for this test case. The viscosity varies according to temperature through Sutherland's law. To force the vortex pairing process, disturbances are added to the initial mean velocity profiles, corresponding to a fundamental and a subharmonic disturbance:

$$\begin{cases} u' = \sum_{k=1}^2 a_k \frac{yL_x}{k\pi b} \cos(2\pi kx/L_x) \exp(-y^2/b) \\ v' = \sum_{k=1}^2 a_k \sin(2\pi kx/L_x) \exp(-y^2/b) \end{cases} \quad (27)$$

where  $L_x$  is the box length in the x-direction,  $b = 10$  is the y-modulation,  $a_1$  and  $a_2$  are the amplitudes of the disturbances. This provide a standard divergence-free disturbance to the mixing layer in an efficiently excited mode.

The rectangular computational domain is meshed using the same Cartesian grid technique used in [25], with equally spaced nodes in the x-direction and stretched in the y-direction, using the mapping

$$y = \frac{L_y}{2} \frac{\sinh(b_y \eta)}{\sinh(b_y)} \quad (28)$$

where  $b_y$  is a stretching factor. The equally spaced mapped coordinate  $\eta$  runs from -1 to +1. Periodic boundary conditions in the x-direction are used and slip wall boundary conditions are imposed in the y-direction.

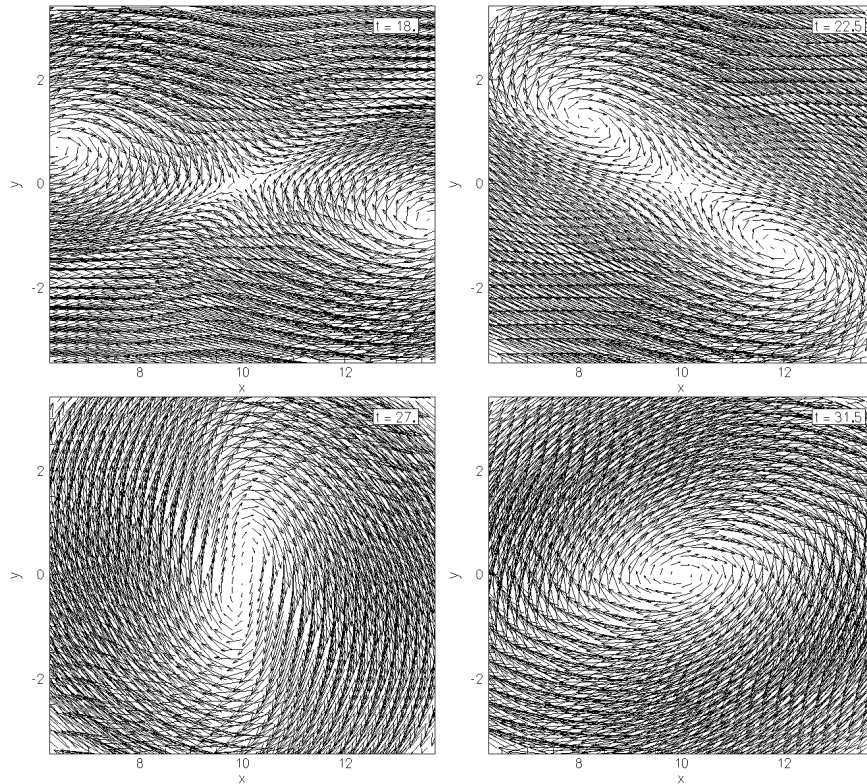
The amplitudes of the disturbances are  $a_1 = 0.025$  and  $a_2 = 0.05$ ,  $L_x = L_y = 20$  are the box length in the x and y directions and  $b_y = 2.4$  is the stretching factor. We compute this test case on a 101 x 101 grid.

We refer to Sandham [18] for a fine analysis of the vortex pairing process for that fully subsonic flow. A pair of co-rotating vortices take place which rotate one over the other, while elongating before pairing.

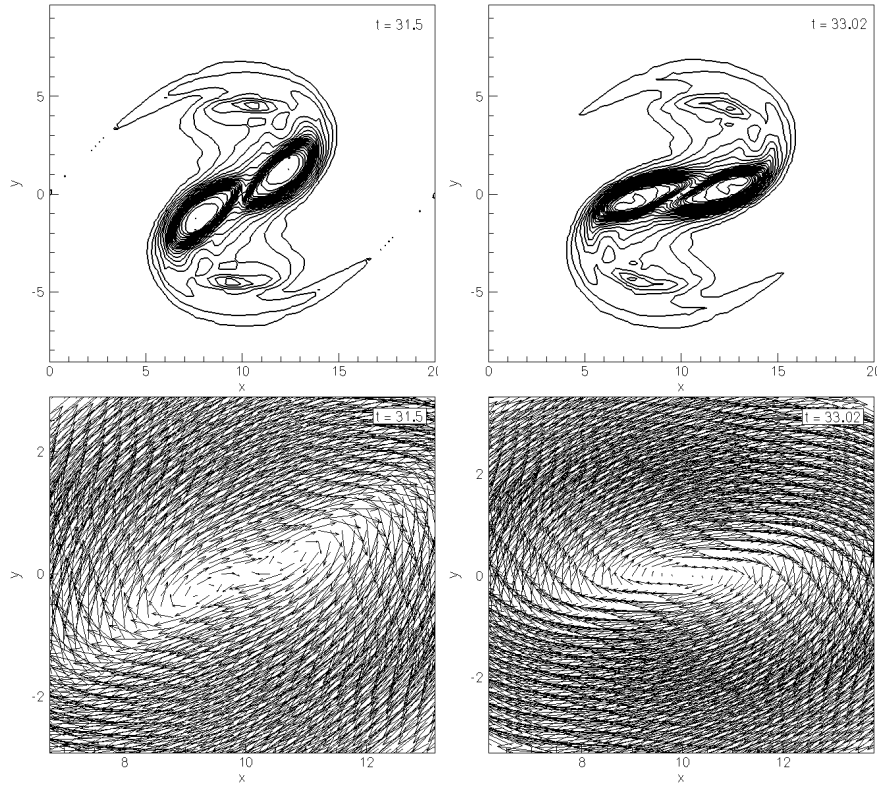
The present results in Fig. 7 compare very well with those presented in [18]. Fig. 8 shows enlarged snapshots of the velocity field at the same times.

Fig. 9 shows the results obtained with an Euler computation: plotted are the vorticity contours and enlarged snapshots of the velocity field at the estimated time when the vortex pairing occurs for the viscous computation  $t = 31.5$  and the inviscid computation  $t = 33.02$ . The dynamic of the pairing process is globally the same

in a viscous or an inviscid computation due to the numerical viscosity of the scheme, but the characteristic times differ quickly. In particular, it can be noticed that the viscosity effect is first to delay the pairing time and then to diffuse the vorticity, while decreasing the vortex rotation velocity.



**Fig. 8** Vortex pairing in a time-developing mixing layer at  $Mc=0.2$ : time sequence of the velocity field (enlarged view), at times  $t=18, 22.5, 27, 31.5$ , for a  $101 \times 101$  grid (NS computation).



**Fig. 9** Euler computation: time sequence of the vorticity contours (upper) and an enlarged view of the velocity field (down) for the vortex pairing in a mixing layer at  $Mc=0.2$ , at times  $t=31.5$  and  $33.02$  for a  $101 \times 101$  grid.

### 4.3 Laminar flow around a cylinder at low-Reynolds number

This classical 2D test case is that of the flow around a cylinder [9]-[16]. A low Reynolds number based on the diameter  $Re_D = \rho_\infty u_\infty D / \mu_\infty = 500$  was chosen in order to remain below the onset of 3D behavior, and not to have to use limiters. The upstream Mach number is  $M_\infty = 0.33$  and we fix the cylinder diameter  $D = 1$ , the freestream density is  $\rho_\infty = 1$  and velocity is  $u_\infty = 1$ . On outside boundaries are imposed non reflecting boundary conditions.

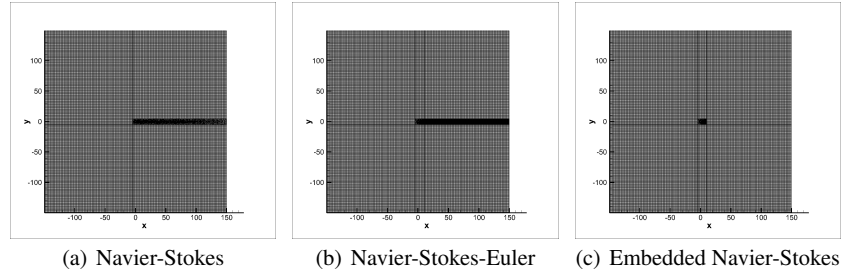


**Fig. 10** Meshes used for computation

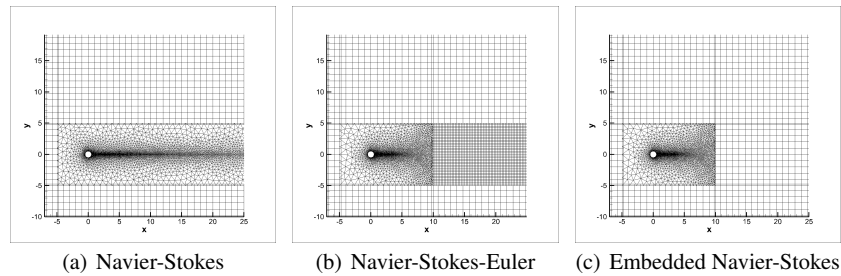


**Fig. 11** Zoom of the three meshes

The first mesh (Navier-Stokes, 10(a), 11(a)) is for a computation where the central domain around the cylinder and the wake are modeled with Navier-Stokes computation on triangles (14000 cells) coupled with the other rectangular domains which are Euler modeled (88400 cells). The second mesh (Navier-Stokes-Euler, 10(b), 11(b)) is for the central domain around the cylinder computed with Navier-Stokes (2544 cells) while the wake is computed with a fine Euler model and the rest of the computational domains are coarser Euler grids. (113000 cells). The third mesh (Embedded Navier-Stokes, 10(c), 11(c)) (4852 cells) is for an embedded Navier-Stokes domain in the center within a global Euler mesh (90000 cells) split into 9 subdomains.

The computation has been run with one to two Schwarz sub-iterations for the Euler-Navier-Stokes computation for time windows the size of 10 Navier-Stokes time steps and 2 to 3 Euler time steps, which allow us to converge to sixth order for each time window. In the embedded Navier-Stokes - Euler computation, the Navier-Stokes domain computes 3 time steps against one time step for the Euler domain.

All three computations give similar instantaneous pressure fields and a Strouhal number of .23.

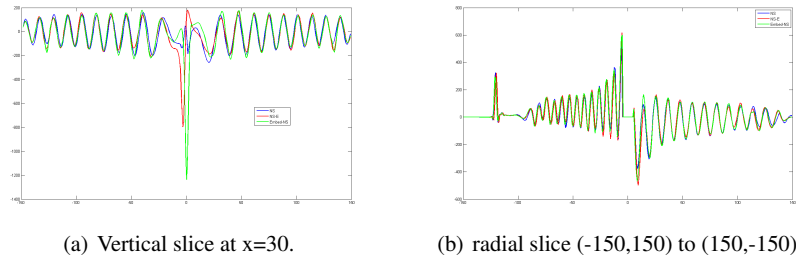


**Fig. 12** Instantaneous acoustic pressure slices at  $T=75$ .

On figures 13 and 14 are shown instantaneous pressure contours. Pressure color scale is between  $-200$  and  $200$ . As is to be expected, the acoustic radiation is almost dipolar.

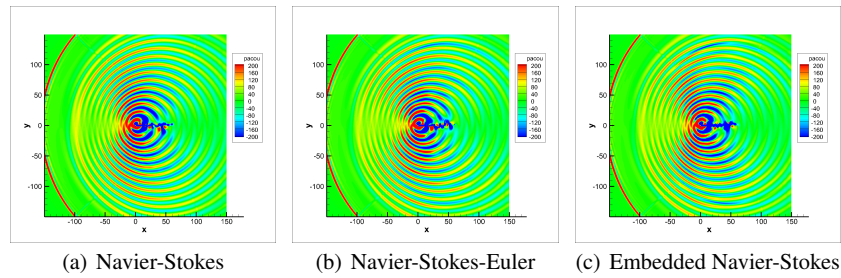


**Fig. 13** Acoustic pressure at  $T=75$ .

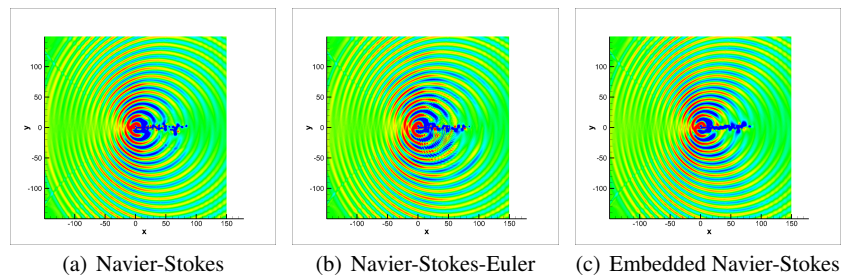


**Fig. 14** Acoustic pressure at  $T=100$ .

At  $T=100$ , a new pressure perturbation appears in the wake for Navier-Stokes Euler computation (slightly weaker in the Navier-Stokes computation).

On figures 15 and 16 are shown vorticity contours for a non dimensioned scale between -1.5 and 1.5. The Von Karman vortex shedding in the near wake are well described. Results for the Navier-stokes wake and the Euler are quite similar , discrepancies occuring with the arrival of the new perturbation in the wake. Vorticity is diffused in the embedded Navier-Stokes Euler computation as the Euler mesh is not fine enough, but this coarseness does not affect the far field acoustic waves.

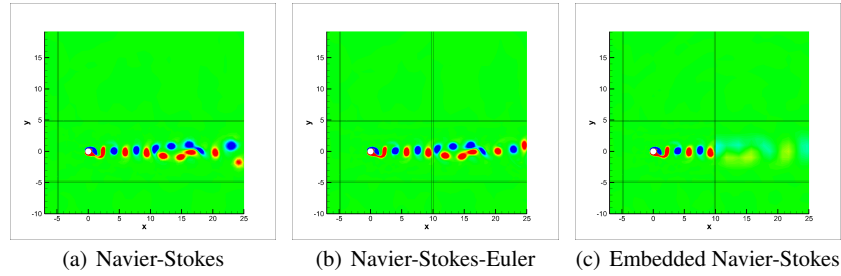


**Fig. 15** Vorticity at T=75.

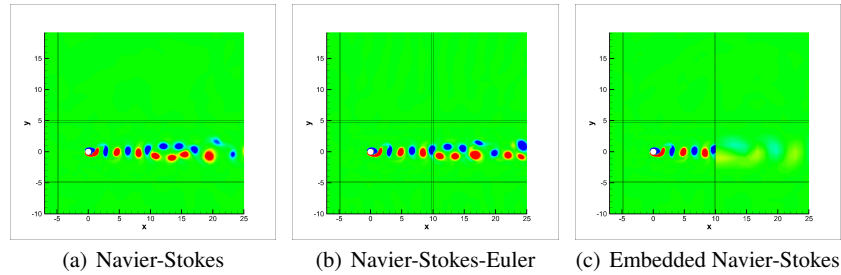


**Fig. 16** Vorticity at T=100.

## 5 Conclusion

Two types of Euler/Navier-Stokes couplings for multiscale aeroacoustic problems have been presented within the framework of DG. The EDG scheme which gives an accurate discretization of the viscous fluxes has been used for the Navier-Stokes computations.

In the EDG scheme, discontinuities are removed at each interface between elements by an  $L^2$  projection on a staggered rectangular element whatever the shape elements is, called elastoplast. We generalized this technique to remove discontinuities, both in space and time, between computational domains due to non conformal grids.

The first two couplings can be interpreted as an interface domain decomposition problem and the third coupling as a volume interpolating problem, but, thanks to the elastoplast technique, all coupling can be implemented in the same manner. The first type of coupling has been numerically evaluated on the test case of the flow around a cylinder at low Reynolds number. As could be done for more complex applications, in 3D for example, we would use Cartesian grids for the acoustic simulations and unstructured meshes for the Navier-Stokes simulations, in particular near the cylinder. This first parallel result shows the interest of the domain decomposition technique in terms of computational cost versus a full Navier-Stokes computation. For very low Reynolds number, optimized transmission condition will have to be defined. Further work will consist in comparing the chimera approach with the Schwarz relaxation technique on a detailed acoustic simulation.

Finally developments will include 3D simulations. For that purpose, the explicit time stepping of the Navier-Stokes solver will be replaced by an implicit one, as for example a space-time DG approach.

## References

1. D'Anfray P., Halpern L. and Ryan J.: *New trends in coupled simulations featuring domain decomposition and metacomputing*, M2AN 36 (5), 953–970 (2002)
2. Bennequin D., Gander M.J. and Halpern L.: *A homographic best approximation problem with application to optimized Schwarz waveform relaxation*, Math. Comp. 78, 185–223 (2009).
3. Borrel M, Halpern L. and Ryan J.: *Euler - Navier-Stokes coupling for Aeroacoustics problems Proceedings of the ICCFD6, St Petersburg (Russia), July 12-16, 2010*, To appear in "Computational Fluid Dynamics 2010" Springer Ed..
4. Borrel M. and Ryan J.: *A new discontinuous Galerkin method for the Navier-Stokes equations*, Proceedings of the ICOSAHOM09, Trondheim (Norway), June 22-26 2009. Published in Lecture Notes in Comp. Sci. and Eng. 76, Hestaven and Ronquist Ed., Springer, pp 373-381.
5. Borrel M. and Ryan J.: *The Elastoplast Discontinuous Galerkin (EDG) Method For The Navier-Stokes Equations*, Submitted to J. Comp. Phys. 2010.
6. Borrel M. and Ryan J.: *A generalized patch AMR platform that uses cell centered or cell vertex solvers*, ECCOMAS CFD conference, 2006; P. Wesseling, E. Onate, J. Periaux Eds, TU Delft, The Netherlands, 2006.
7. Cockburn B. and Shu C.-W.: *The Runge-Kutta discontinuous Galerkin method for conservation laws V: multidimensional systems*, J. Comput. Phys. 141, 199-224 (1998)
8. Desquesnes G. : *Euler Equations in Perturbation 2.5-D: a New System for Acoustic Modal Propagation: 14th AIAA/CEAS Aeroacoustics Conference (29th AIAA Aeroacoustics Conference) 5 - 7 May 2008, Vancouver, British Columbia Canada, AIAA 2008-2822*.
9. Dumbser M.: *Arbitrary high order PNP schemes on unstructured meshes for the compressible Navier-Stokes equations*, Computers & Fluids 39 (2010), 60-76.
10. Gander M.J., Halpern L., Japhet C. and Martin V.: *Viscous Problems with Inviscid Approximations in Subregions: a New Approach Based on Operator Factorization*, ESAIM Proc 27, 272–288 (2009).
11. Gassner G., Lörcher F. and Munz C.-D.: *A contribution to the construction of diffusion fluxes for finite volume and discontinuous Galerkin schemes*, J. Comput. Phys., 224 (2007), pp. 1049-1064.

12. Geuzaine C., Remacle J.F.: *Gmsh: a three-dimensional finite element mesh generator with built-in pre- and post-processing facilities*, *Int. J. for Num. Meth. in Eng.* 79-11, 1309–1331 (2009).
13. Halpern L., Japhet C. and Szeftel J.: *Discontinuous Galerkin and nonconforming in time optimized Schwarz waveform relaxation*, *proceedings of the Eighteenth International Conference on Domain Decomposition Methods*, <http://numerik.mi.fu-berlin.de/DDM/DD18/> (2009).
14. Lelarasmee E., Sangiovanni-Vincentelli A.L. and Ruehli A.E.: *The waveform relaxation method for time-domain analysis of large scale integrated circuits*, *IEEE Trans. on Computer-Aided Design of Integrated Circuits and Systems*, vol. CAD-1, 131–145 (1982).
15. Lions P.-L.: *On the Schwarz alternating method. I.*: In Roland Glowinski, Gene H. Golub, Gérard A. Meurant, and Jacques Périaux, editors, *First International Symposium on Domain Decomposition Methods for Partial Differential Equations*, *SIAM*, 1–42 (1988).
16. Marsden O., Bogey C. and Bailly C. : *High-order curvilinear simulations of flows around non-cartesian bodies*, *Journal of Computational Acoustics*, Vol. 13, No. 4 (2005) 731748.
17. Penel Y., Mekkas A., Dellacherie S., Ryan J. and Borrel M.: *Application of an AMR strategy to an abstract bubble vibration model*, *AIAA paper 2009-3891*, 19<sup>th</sup> CFD Conf., San Antonio, Texas.
18. Sandham N.D., *The effect of compressibility on vortex pairing*, *Phys. Fluids* 6 (2), February 1994.
19. Schwarz H. A. Über einen Grenzübergang durch alternierendes Verfahren. *Vierteljahrsschrift der Naturforschenden Gesellschaft in Zürich*, 15, 272–286 (1870).
20. Shu C.-W. ,Osher S.: *Efficient implementation of essentially non-oscillatory shock-capturing schemes*, *J. Comput. Phys.* 77 , 439-471 (1988).
21. Toro E. F. , Spruce M., Speares W.: *Restoration of the contact surface in the HLL-Riemann solver*, *Shock Waves* 4, , 2534 (1994).
22. Utzmann J., F. Lorcher F., M. Dumbser M. and C.D. Munz C.-D.: *Aeroacoustic Simulations for Complex Geometries based on Hybrid Meshes*, *AIAA paper 2006-2418*, May 2005.
23. B. van Leer and Nomura S.: *Discontinuous Galerkin Method for Diffusion*, *AIAA paper 2005-2108*, June 2005.
24. B. van Leer and Lo M.: *A Discontinuous Galerkin Method for Diffusion Based on Recovery*, *AIAA paper 2007-4003*, 18<sup>th</sup> CFD Conf., Miami.
25. Yee H.C., Sandham N.D. and Djomehri J.: . *Low-dissipative high-order shock-capturing methods using characteristic-based filters*, *J. Comp. Phys.*, flight 150, pp.199–238 (1999).